Electronic Supplementary Material (ESI) for Journal of Materials Chemistry B
This journal is © The Royal Society of Chemistry 2019

Supplementary Information

Polymer Microneedles with Interconnected Porous Structure via Phase Inversion Route for Transdermal Medical Applications

Pei Liu,[‡a] Hongyao Du,[‡b] Yu Chen,[a] Hua Wang,[a] Jinzhu Mao,[b] Lianbin Zhang,*[a] Juan Tao[b] and Jintao Zhu*[a]

[a] *Key Laboratory of Material Chemistry for Energy Conversion and Storage of Ministry of Education (HUST), and State Key Laboratory of Materials Processing and Mold Technology, School of Chemistry and Chemical Engineering, Huazhong University of Science and Technology (HUST), Wuhan 430074, China. E-mail: zhanglianbin@hust.edu.cn (L. Z.); jtzhu@mail.hust.edu.cn (J. Z.).*
[b] *Department of Dermatology, Union Hospital, Tongji Medical College, HUST, Wuhan 430022, China.*

Supplementary Figures:

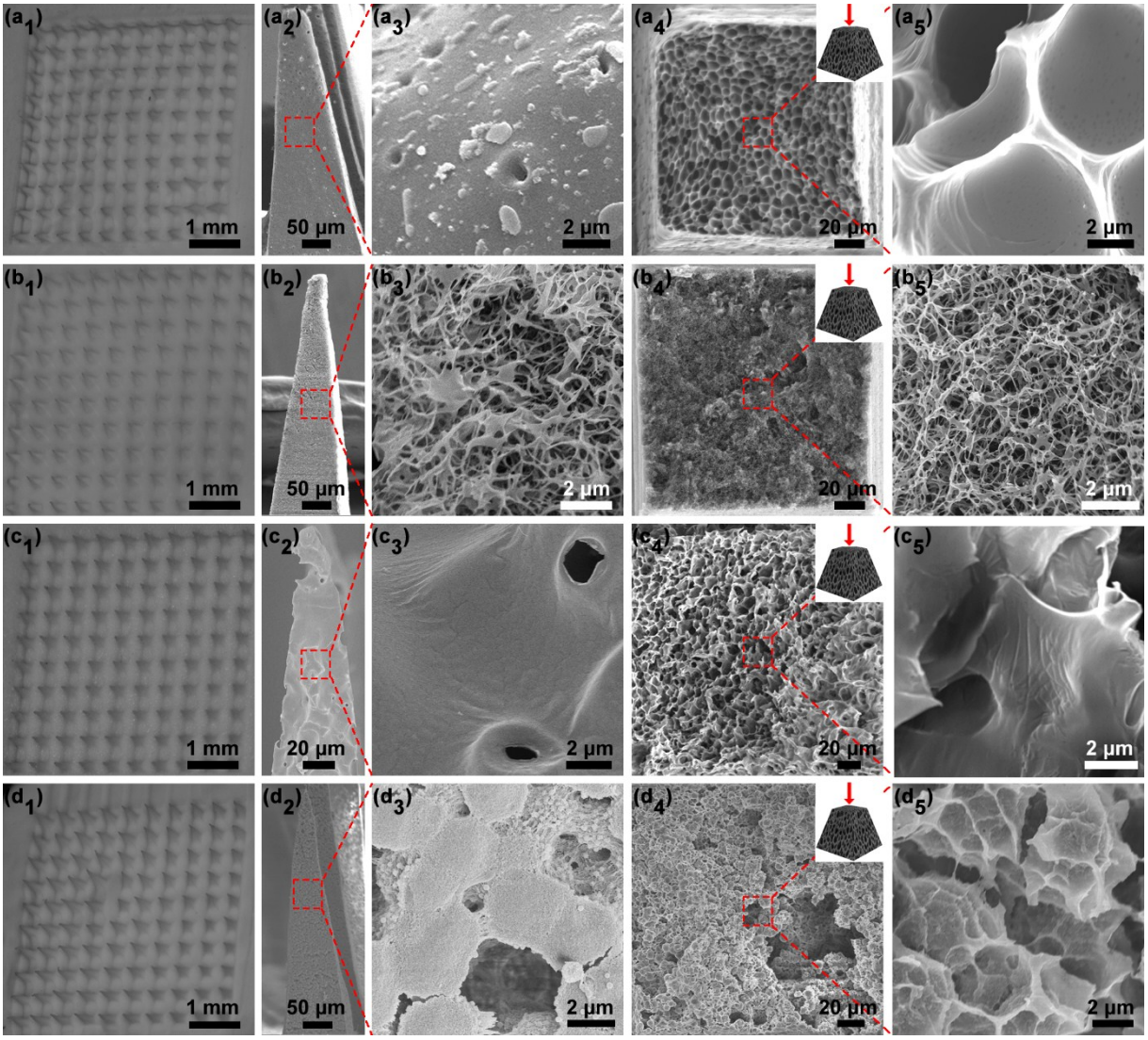

Fig. S1 Characterization of porous microneedles (MNs) made of PES (a_1 ~ a_5), PLGA (b_1 ~ b_5), PLA (c_1 ~ c_5), and PVDF (d_1 ~ d_5), respectively. Optical microscopy images of the MN arrays (a_1 ~ d_1). Surface (a_2 ~ d_2 and a_3 ~ d_3) and cross-sectional (a_4 ~ d_4 and a_5 ~ d_5) SEM images of PES, PLGA, PLA and PVDF MNs with different magnifications. The optical microscopy images show that MNs with good tapered structure and sharp needles could be prepared. Surface and cross-sectional scanning electron microscope (SEM) images of single needle demonstrated that porous structure with interconnected pores is obtained.

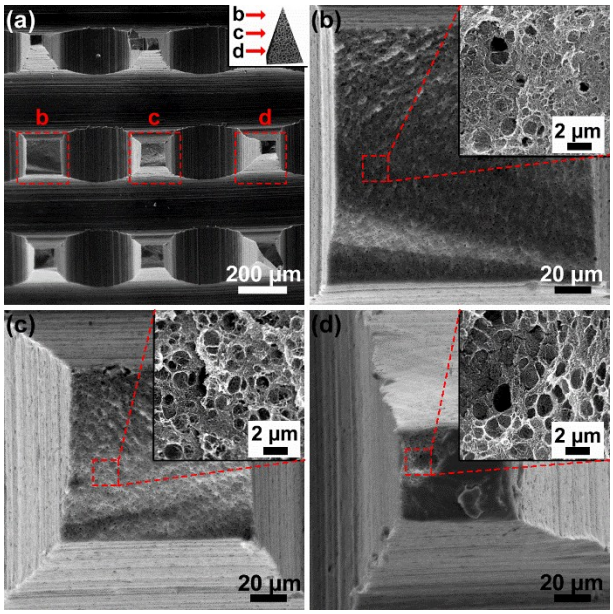

Fig. S2 Cross-sectional SEM images of CA MNs made of 35 wt % CA solution at different position of the MNs. Inset in (a) shows the schematic illustration of the cross-sectional position of the MNs in (b-d). It can be observed that the microstructures throughout the needles are consistent.

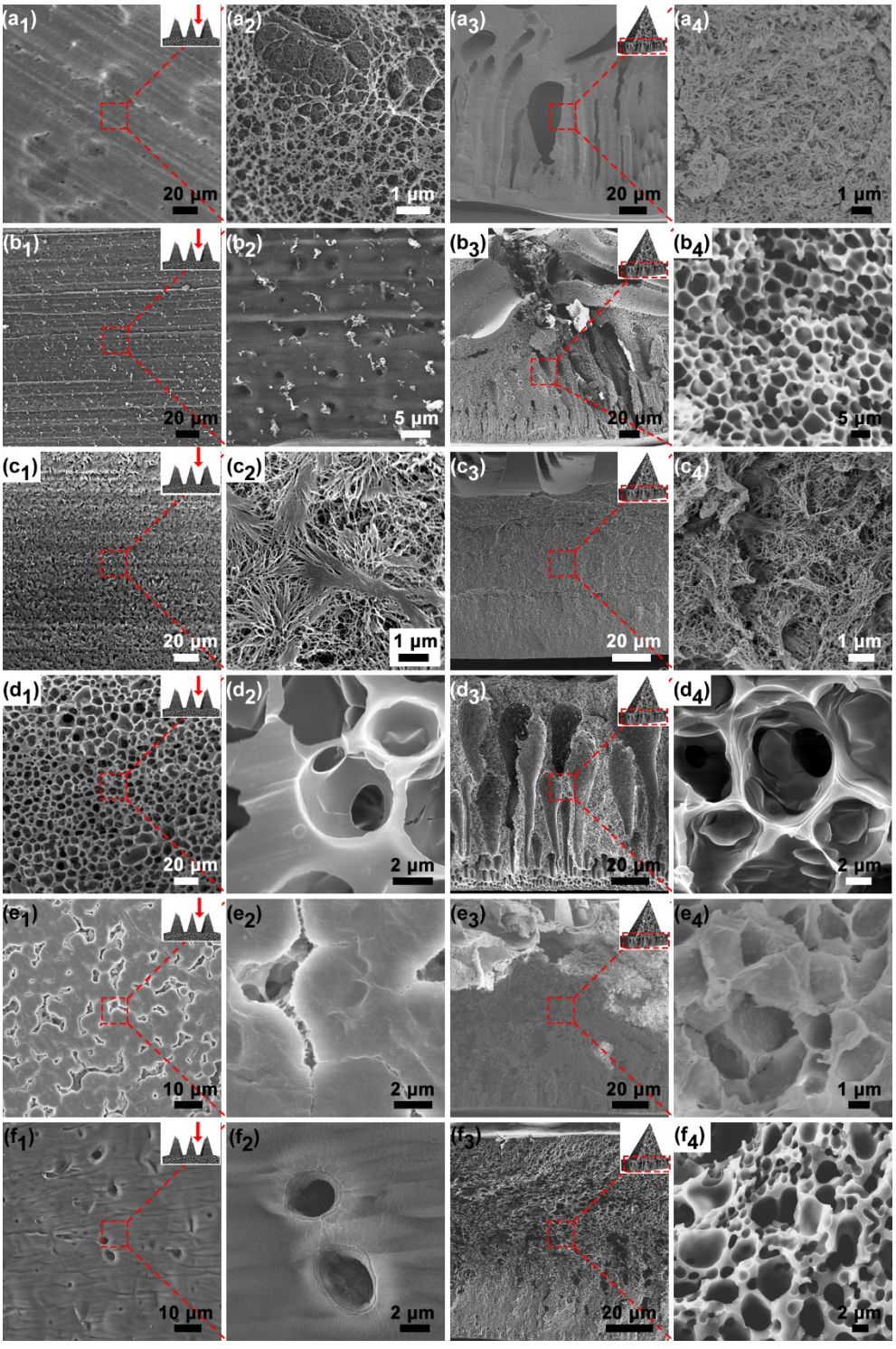

Fig. S3 Characterization of porous MNs made of CA (a_1 ~ a_4), PES (b_1 ~ b_4), PLGA (c_1 ~ c_4), PLA (d_1 ~ d_4), PVDF (e_1 ~ e_4), and PSF (f_1 ~ f_4), respectively. Surface (a_1 ~ f_1 and a_2 ~ f_2) and cross-sectional (a_3 ~ f_3 and a_4 ~ f_4) SEM images of the base of CA, PES, PLGA, PLA, PVDF and PSF MNs with different magnifications.

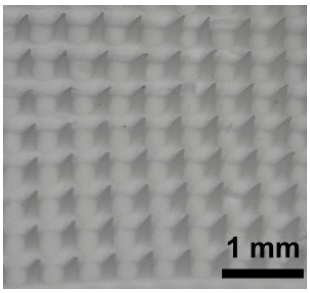

Fig. S4 Optical microscopy image of CA MN after 1 year. The morphology of CA MN remained unchanged, indicating the good stability of the CA MN.

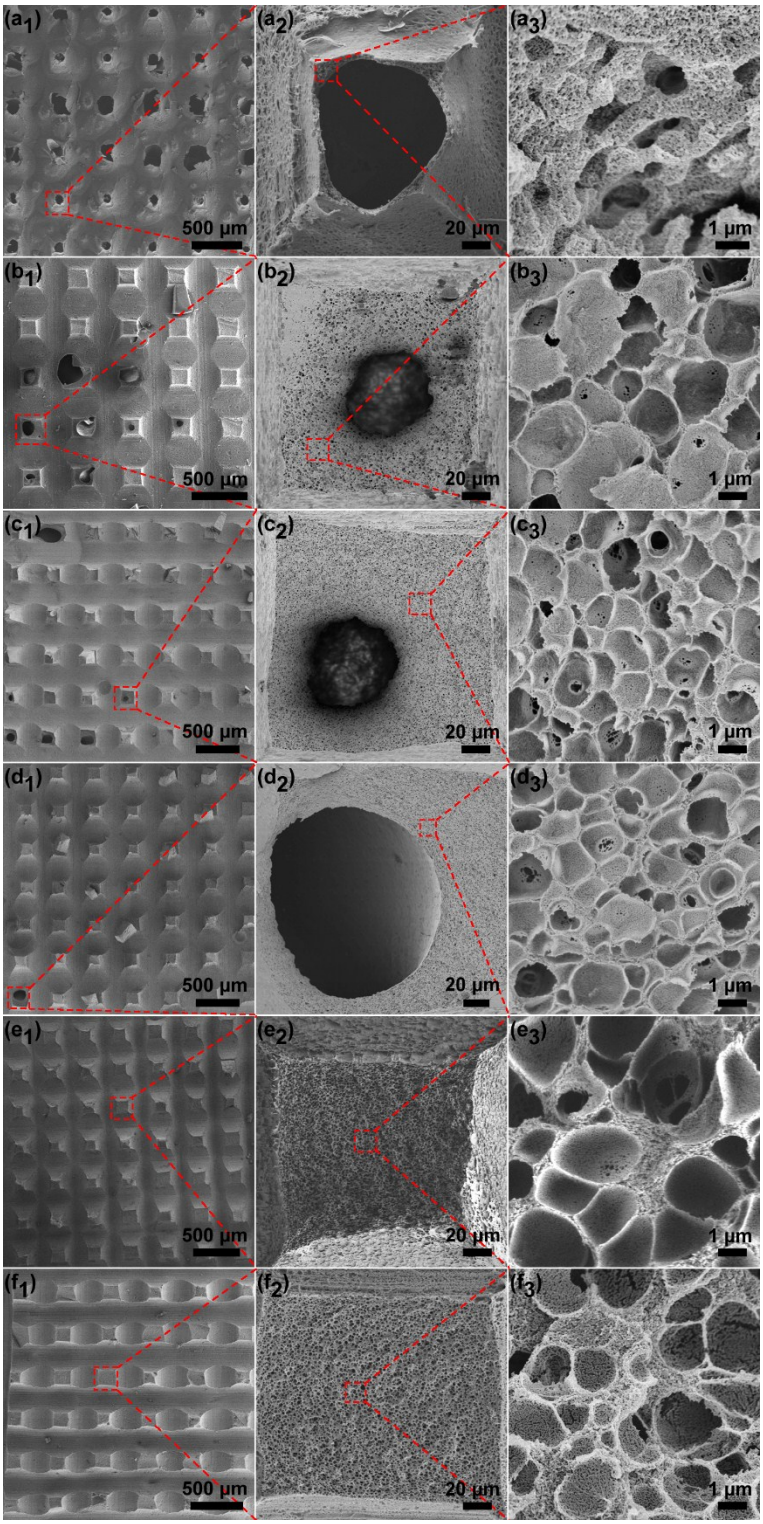

Fig. S5 Cross-sectional SEM images with varying magnifications of porous CA MNs made of different initial concentrations: 10 wt % (a_1 ~ a_3), 15 wt % (b_1 ~ b_3), 20 wt % (c_1 ~ c_3), 25 wt % (d_1 ~ d_3), 30 wt % (e_1 ~ e_3), 35 wt % (f_1 ~ f_3), respectively.

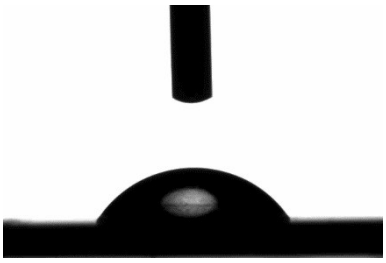

Fig. S6 The water contact angle of a smooth CA film obtained by spin-coating.

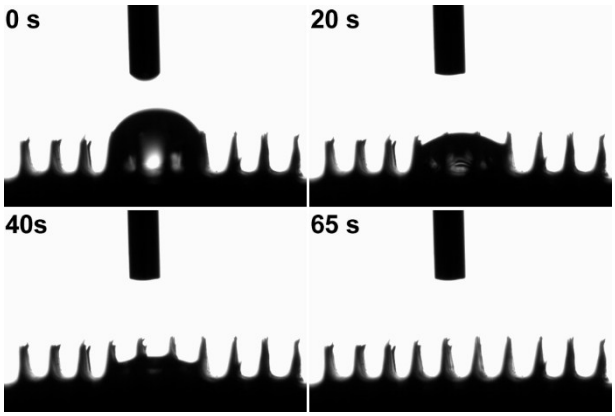

Fig. S7 Snapshots shows the water spreading process on the porous CA MN over time. Water droplet with the size of 2 µL spread over the surface within 65 s, indicating that water can be absorbed by porous CA rapidly.

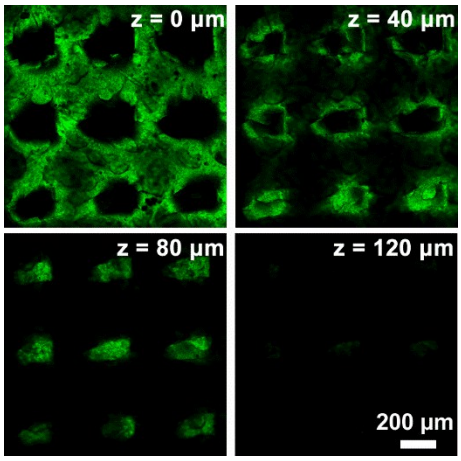

Fig. S8 Confocal laser scanning microscopy (CLSM) images of porcine cadaver skin after administration of sodium fluorescein-loaded CA MN made of 35 wt % CA solution for 10 min. The scale bars can be applied to the other images. The CLSM images show that CA MN could penetrate the stratum corneum and reach the dermis.

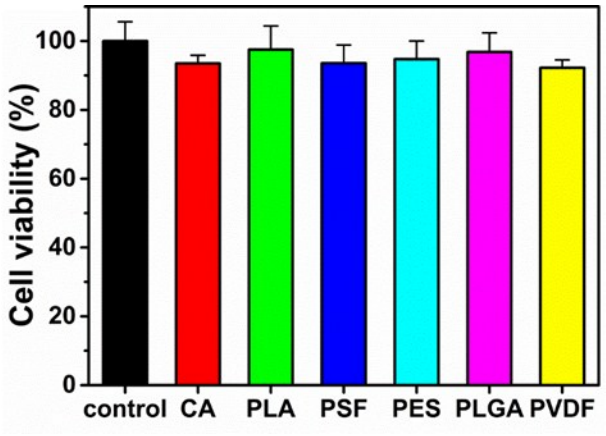

Fig. S9 The cytotoxicity study of the MNs made of different polymer materials. The MNs were incubated with NIH-3T3 fibroblasts for 24 h.

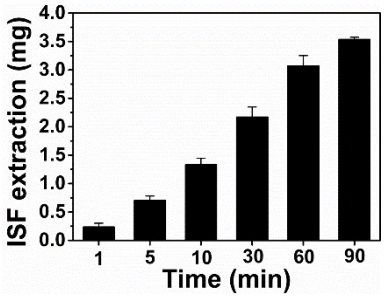

Fig. S10 The ISF extraction amount of CA MNs over time in mice. The increase of mass indicates the diffusion of ISF from the skin to MNs.